Journal of Solid State Chemistry 322 (2023) 123969

Contents lists available at ScienceDirect

Journal of Solid State Chemistry

journal homepage: www.elsevier.com/locate/jssc

$CaPt_4P_6$, first calcium-containing representative of the ternary pyrite-derived pnictides of the $BaPt_4As_6$ type: Synthesis, crystal, and electronic structure

Anastasiya Yu Makhaneva [a], Elena Yu Zakharova [a], Sergey N. Nesterenko [a], Konstantin A. Lyssenko [a,b], Alexey N. Kuznetsov [a,*]

[a] Department of Chemistry, Lomonosov Moscow State University, Leninskie Gory 1-3, 119991, Moscow, Russia
[b] National Research University Higher School of Economics, Miasnitskaya Str. 20, 101000, Moscow, Russian Federation

ARTICLE INFO

Keywords:
Phosphides
Platinum-rich compounds
Flux-assisted crystal growth
Crystal structure
DFT calculations
Chemical bonding

ABSTRACT

Mixed calcium-platinum phosphide $CaPt_4P_6$ was synthesized using flux-assisted high-temperature ampoule technique. According to single-crystal XRD data it crystallizes in the monoclinic space group $C2/c$ with $Z = 4$ (a = 8.1361(3) Å, b = 7.9489(3) Å, c = 11.3803(5) Å, β = 90.860(2)°, $R_1 = 0.0240$, $wR_2 = 0.0618$) and belongs to the $BaPt_4As_6$ structure type, the structure of which is derived from pyrite structure where one atom of alkaline earth metal per formula unit occupies P_2-unit position. DFT calculations predict all known representatives of the $BaPt_4As_6$ structure type to be narrow-gap semiconductors (calculated bandgap values are: 0.43 eV ($CaPt_4P_6$), 0.57 eV ($SrPt_4P_6$), 0.27 eV ($SrPt_4As_6$) and 0.40 eV ($BaPt_4As_6$)). Bonding analysis establishes that all these compounds are based on the 3D framework of the Pt-Pn and Pn-Pn interactions, with AE cations occupying the voids with varying degree of the distortion of the AE coordination.

1. Introduction

Chemistry of pnictogens is no doubt one of the most complex, but also one of the most engaging among the groups in the Periodic Table. Both the elements themselves and their binary and more complex (ternary and higher order) compounds show a great variety of compositions, structures and, naturally, manifested physical properties [1–3]. Pnictide chemistry has been one of the rapidly developing fields in the last couple of decades and the level of knowledge relating to the chemistry of phosphides, arsenides, antimonides, and bismuthides has increased enormously and has led to great progress in terms of understanding the structure-property relationships and potential applications of said compounds in such key areas as energy storage and conversion, hydrogen storage, thermoelectricity and photocatalysis for hydrogen production [1,4–7].

Of particular interest is chemistry of pnictides, because to date they represent a relatively understudied class of inorganic compounds, as compared to ubiquitous oxides. Perhaps, the most studied up to date are iron phosphides and arsenides, due to their relatively recently discovered high-temperature superconductivity [8,9]. Other fairly large areas of research are phosphides of rare-earth and transition elements, phosphide oxides, metal-rich phosphides and polyphosphides. Although many such compounds, both binary and more complex, have been obtained, with completely different compositions and structures, there are still many blank spaces in the chemistry of phosphides [10–12].

If we consider ternary systems consisting of an alkaline earth element, a group 10 metal, and phosphorus, we notice, that among a huge variety of compounds known in these systems [13], rather few compounds with high phosphorus content (≥50 at. %) are encountered, albeit they show an unexpected richness of chemical compositions, physical properties and structural features. No other element comes close to phosphorus in the variety of formed homoatomic polyanions, the result of its relatively low electronegativity and stereochemical features [10]. Such compounds include phases of composition 1:2:4, 1:2:3, 2:1:3, and 1:4:6. These are the compounds like $BaPd_2P_4$ [14], $SrNi_2P_4$ [15], β-$BaNi_2P_4$ [16], $BaPt_2P_3$ [17] and Ba_2PdP_3 [14] that crystallize in their own structure types; α-$BaNi_2P_4$ isotypic to $BaPd_2P_4$ [16], and $SrPt_4P_6$ which crystallizes in the $BaPt_4As_6$ structure type [17]. It is worth noting that the latter structure type is rather rare, as only three compounds belong to it.

In this paper we report on the synthesis and characterization of the

* Corresponding author.
E-mail address: alexei@inorg.chem.msu.ru (A.N. Kuznetsov).

https://doi.org/10.1016/j.jssc.2023.123969
Received 21 January 2023; Received in revised form 2 March 2023; Accepted 5 March 2023
Available online 11 March 2023

crystal and electronic structure as well as the chemical bonding of a new ternary platinum-calcium phosphide $CaPt_4P_6$, which becomes a first representative of the $BaPt_4As_6$ structure type containing calcium.

2. Materials and methods

2.1. Synthesis and crystal growth

The $CaPt_4P_6$ compound was obtained during exploratory synthesis of new quaternary phosphide platinides of the $Eu_2Pt_7AlP_{2.95}$ type, which are the intergrowth structures of $AuCu_3$ and $CaBe_2Ge_2$-type blocks, in Ca–Pt-X-P systems, where X = Al, Ti [18]. Calcium (granules, 99%), platinum (ingots, 99.97%), titanium (ingots, 99.99%), aluminum (flakes, 99.999%) metals and red phosphorus (powder, 99.9%) were used in the process. Single crystals were grown using a high-temperature ampoule technique and lead metal (ingots, 99.99%) as a flux. Elemental substances mixed in a molar ratio Ca:Pt:X:P (X = Al, Ti) equal to 2:7:1:3, as well as a 10 x molar excess of lead with respect to the calcium amount, were placed in corundum crucibles. The total weight of the target elements was ca. 0.5 g, with the weight of lead ca. 1–2 g, depending on the other components. The crucibles were then put into vacuum-dried silica ampoules with silica wool on top. The corundum crucibles and silica wool were pre-dried at 800 °C before use.

The ampoules were then washed three times with pure dry argon and then sealed off at the internal argon pressure of 200 Torr at room temperature. In the case of the aluminum-containing sample, the ampoule was then annealed at 1050 °C for 120 h and slowly (ca. 5°/h) cooled down to 300 °C, after which it was allowed to cool down to room temperature naturally. For the titanium-containing sample, the annealing time was 24 h at 1050 °C, then slow cooling (ca. 1°/h) down to 900 °C, and then down to 600 °C at ca. 5°/h and down to room temperature naturally. Single crystals were separated from the flux by centrifugation through a silica wool (Hettich EBA-200 laboratory centrifuge) at 550 °C. Crystals of the new ternary phosphide $CaPt_4P_6$ were obtained from both aluminum- and titanium-containing samples in a form of grey thick plates with a metallic lustre, stable in air.

It is worth noting that the other three representatives of the $BaPt_4As_6$ structure type containing strontium and barium, were obtained, as reported in the literature [17], by direct high-temperature ampoule synthesis from the elements in an argon atmosphere at 1000–1050 °C using a small excess of alkaline earth metal. In the case of our calcium-containing compound, we used a flux-assisted technique of crystal growth to obtain and characterize its crystals. This phase, however, was also observed by us as one of the products of direct high-temperature synthesis of the bulk samples and also as an impurity in the synthesis of the Ca–Pt-X-P samples in several systems. However, as direct synthesis from the elements always lead to multi-phase products in 7–12 days of annealing, we chose not to further pursue this route.

2.2. Sample characterization

The composition of the crystals was determined using the energy dispersive X-ray spectroscopy (EDX). A scanning electron microscope JSM JEOL 6490 LV equipped with an energy dispersive X-ray detection system INCA x-Sight (Oxford Instruments) was used for the analysis of chemical composition. Acceleration voltage was set at 30 kV, average spectrum collection time ca. 40 s. For each sample, 5 to 7 crystals were analyzed with 3–10 points per crystal. EDX data has shown no traces of either lead or titanium or aluminum in the crystals. The average composition of the crystals was $Ca_{1.00(5)}Pt_{3.95(7)}P_{5.98(8)}$. The details of the EDX analysis are provided in the Supplementary Materials.

2.3. Crystal structure determination

Single crystals of the $CaPt_4P_6$ compound, obtained from the sample in the Ca–Pt–Ti–P–Pb system, were investigated on a Bruker D8 QUEST single-crystal X-ray diffractometer equipped with PHOTON II detector, charge-integrating pixel array detector (CPAD), laterally graded multilayer (Goebel) mirror and microfocus Mo-target X-ray tube (λ = 0.73071 Å). The frame width of 0.4° and exposure time of 1.5 s per frame were employed for data collection. Data reduction and integration were performed with the Bruker software package SAINT (Version 8.40B) [19]. The data were corrected for Lorentz and polarization effects.

Table 1
Selected crystallographic data and refinement parameters for $CaPt_4P_6$ from single crystal X-ray diffraction.

Chemical formula	$CaPt_4P_6$
Formula mass, g mol^{-1}	1006.26
Crystal system	monoclinic
Space group	*C2/c (No.15)*
a, Å	8.1361(3)
b, Å	7.9489(3)
c, Å	11.3803(5)
β, °	90.860(2)
V, Å^3	735.92(5)
Z	4
T, K	130(2)
$d_{calcd.}$, g cm^3	9.082
μ, mm^{-1}	77.699
θ range, °	$3.581 < \theta < 26.480$
Collected reflections	4065
Independent reflections	755
R_σ/R_{int}	0.0405/0.0546
Reflections with$I > 2\sigma(I)$	736
Refined parameters	55
Largest difference peak/hole, e Å^{-3}	2.179/-1.542
R_1 [$I > 2\sigma(I)$]/R_1 [all data]	0.0240/0.0246
wR_2 [$I > 2\sigma(I)$]/wR_2 [all data]	0.0618/0.0622
GoF	0.911

The absorption correction was performed using multiscan routine as implemented in SADABS (Version 2016/2) [20]. The *μr* value (where *μ* is the linear absorption coefficient and r is the effective radius of the crystal) was selected in interactive mode by the gradual increase of the *μr* value from the minimum dimension of the crystal towards the maximum one. Crystal structure solution and refinement were performed using SHELX-2018 package [21]. Atomic positions were located using direct methods and refined using a combination of Fourier synthesis and least-square refinement in isotropic and anisotropic approximations. Crystallographic parameters and final residuals for the single-crystal XRD experiments are given in Table 1. A summary of crystallographic data for the single-crystal experiments is available from CCDC, ref. number 2232623.

2.4. Electronic structure calculations

DFT calculations on the electronic structure of synthesized $CaPt_4P_6$, as well as previously reported $SrPt_4Pn_6$ (Pn = P, As) and $BaPt_4As_6$ were performed using the projector augmented wave method (PAW) as implemented in the *Vienna Ab initio Simulation Package* (VASP) [22,23]. Experimental structures were used for the modelling and were transformed to the *P*1 group for the calculations; in all cases, the relaxation of atomic coordinates was carried out to eliminate structural tension. The r^{2}SCAN exchange-correlation functional of the meta-GGA type was used for the calculations [24,25]. The number of *k*-points in the first Brillouin zone was chosen so as to provide a step between k-points of no more than 0.02 Å^{-1}. Energy cutoff was set to 500 eV, and the energy convergence criterion was at 10^{-5} eV. Convergence towards the *k*-point set and energy was checked. ELF (Electron Localization Function) and charge density analyses were performed using Multiwfn 3.8 package [26]. ELF topology was visualized using VESTA 3.5.7 package [27]. DOS and band plots were produced using sumo 2.3.5 package [28]. Crystal orbital Hamiltonian population analysis was performed using LOBSTER 4.1.0 package [29–32].

Table 2
Fractional atomic coordinates and isotropic displacement parameters for $CaPt_4P_6$.

Atom	Wyckoff site	x/a	y/b	z/c	U_{eq}[a], Å^2
Pt1	8f	0.21517(5)	0.29058(5)	0.25024(3)	0.01109(19)
Pt2	4a	0	0	0	0.0108(2)
Pt3	4b	0	½	0	0.0113(2)
Ca	4e	0	0.5950(3)	¼	0.0107(5)
P1	8f	0.2515(3)	0.3648(3)	0.0537(2)	0.0126(5)
P2	8f	0.1367(4)	0.2532(3)	0.4489(2)	0.0125(5)
P3	8f	0.1109(3)	0.0195(3)	0.1949(2)	0.0127(5)

[a] U_{eq} is defined as one third of the trace of the orthogonalized U_{ij} tensor.

Table 3
Selected interatomic distances for $CaPt_4P_6$.

Atoms		Distance, Å	Atoms		Distance, Å
Pt1 -	P1	2.336(2)	**Pt3 -**	P2	2.333(3)
	P2	2.377(3)		P1	2.383(2)
	P3	2.382(2)		Ca	2.9436(7)
	P3	2.397(3)	**Ca -**	P3	3.273(3)
	Ca	2.7905(15)		P3	3.551(4)
	Ca	2.987(2)		P1	3.559(3)
Pt2 -	P2	2.376(3)	**P1 -**	P1	2.196(5)
	P1	2.378(2)	**P2 -**	P2	2.166(6)
	P3	2.387(3)	**P3 -**	P3	2.213(5)

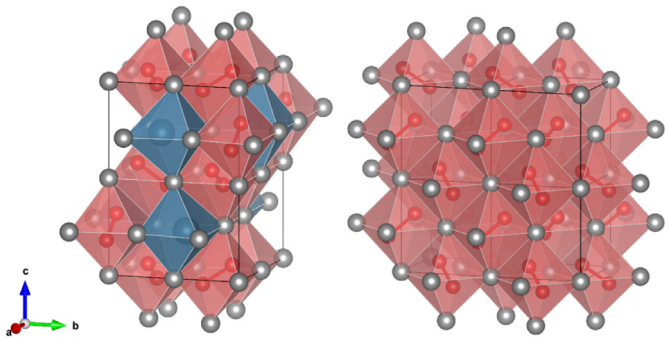

Fig. 1. The crystal structure of $CaPt_4P_6$ (left) and PtP_2 (right) with highlighted octahedra formed by platinum atoms (blue ones are Ca-centered, pink ones are P_2-centered). Ca atoms are light blue, Pt – grey, and P - red.

3. Results and discussion

3.1. Characterization and crystal structure description

According to the EDX data, the composition of the crystals of the ternary phase obtained from lead flux correspond to the $CaPt_4P_6$ formula with excellent agreement. EDX data also confirms that the compound is ternary and does not contain any measurable Ti, Al, or Pb impurities. The structure of the compound was determined by X-ray diffraction on a single crystal grown from lead flux in the Ca–Pt–Ti–P system. Based on X-ray diffraction data, the compound $CaPt_4P_6$ crystallizes in monoclinic crystal system (space group *C*2/*c*) and belongs to the $BaPt_4As_6$ structure type. Atomic coordinates, isotropic displacement parameters, and selected interatomic distances for the $CaPt_4P_6$ compound are given in Tables 2 and 3.

As we mentioned above, up to now there have only been three compounds of this type according to the literature data: $SrPt_4P_6$, $SrPt_4As_6$, and $BaPt_4As_6$ [17], and thus the title compound represents the first calcium-containing compound of this type. The structures of these ternary pnictides can be considered as a derivative of PtP_2 or $PtAs_2$ (pyrite type FeS_2, space group *Pa*-3) [33], in which one AE (alkaline earth metal) atom per formula unit takes the position of the P_2 or As_2 pair (see

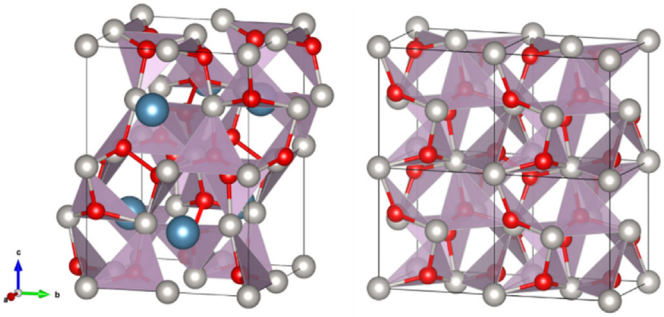

Fig. 2. Crystal structures of $CaPt_4P_6$ (left) and PtP_2 (right) in the polyhedral representation. Ca atoms are shown in light blue, Pt in grey, and P in red.

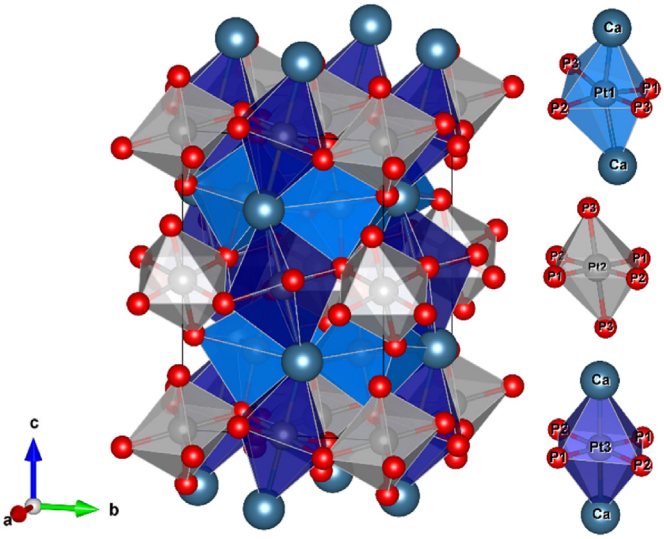

Fig. 3. Unit cell of $CaPt_4P_6$ in the polyhedral representation (left), and types of the coordination polyhedra of Pt (right).

Fig. 1). The remaining three Pn_2 dumbbells (Pn = P, As), as these units are traditionally considered, coordinated by six Pt atoms represent original fragments of the pyrite structure. The bond lengths inside the P–P dumbbells within $CaPt_4P_6$ are 2.17–2.22 Å, and in another known phosphide, $SrPt_4P_6$, P–P distances were found to be almost identical, 2.17–2.24 Å, which approximately matches the sum of covalent radii of 2.20 Å [34]. These values are in good agreement with the values obtained for the binary phosphide PtP_2, where average P – P distances are 2.22 Å.

In the PtP_2 structure platinum atoms form a framework with octahedral voids, all these voids are filled with P_2 dumbbells, which have various orientation (Fig. 1, right). In the structure of $CaPt_4P_6$, the "ideal" platinum sublattice is distorted due to the replacement of one fourth of the phosphorus pairs in the cell by calcium atoms. This causes platinum to shift from its ideal position (as it should be in a *fcc* NaCl type lattice), leading to lower symmetry, so the octahedra formed by the platinum atoms become slightly distorted (Fig. 1, left).

Thus, while in the structure of the binary phosphide the centres of the P_2 units were located exactly in the middle of the edges, as well as in the centre of the unit cell, in the structure of $CaPt_4P_6$, where some dumbbells are replaced by calcium atoms, these calcium atoms do not sit exactly in the middle of the edges anymore. Moreover, this replacement of the P_2 units by calcium atoms causes a slight reorientation of the remaining P_2 units.

Also, in the structure of $CaPt_4P_6$ it is possible to arbitrarily select {PPt_3} distorted trigonal pyramids which have a phosphorus atom in the vertex (Fig. 2, left). Similar polyhedra are observed in PtP_2 (Fig. 2, right),

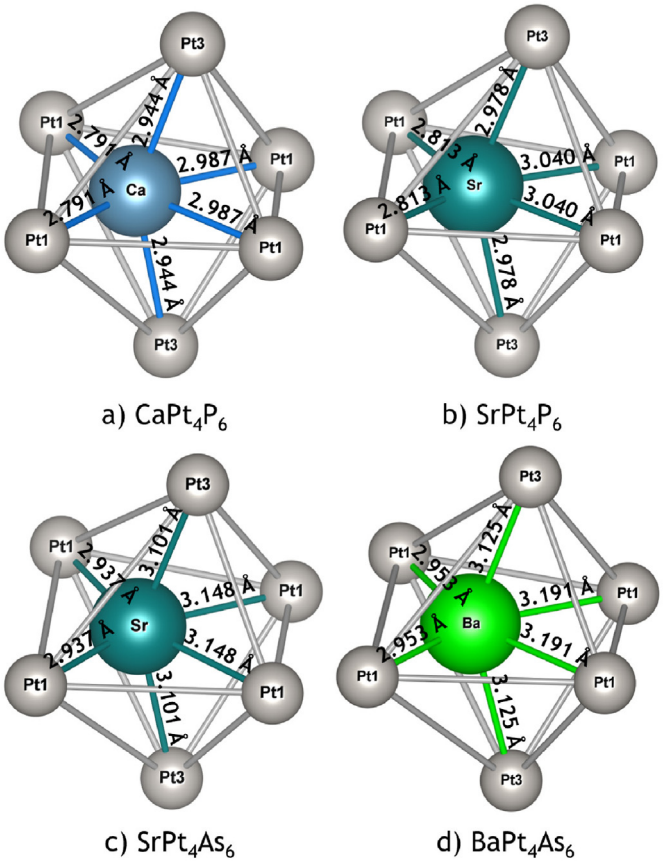

Fig. 4. AE-Pt distances in structures of $CaPt_4P_6$ (a), $SrPt_4P_6$ (b), $SrPt_4As_6$ (c), and $BaPt_4As_6$ (d).

where each phosphorus atom has one phosphorus atom and three platinum atoms as the nearest atoms in a distorted tetrahedral environment. Trigonal pyramids are connected through platinum atoms located in the vertices. The Pt - P distances are in the range of 2.33–2.40 Å. For the comparison, in the binary platinum phosphide of the pyrite type PtP_2 these distances are 2.39 Å.

In the binary phosphide PtP_2 platinum atoms are in a perfect octahedral environment of phosphorus atoms. In the $CaPt_4P_6$ structure, on the other hand, platinum atoms occupy three crystallographically independent positions, and only one of them keeps their environment: Pt2 atoms are located in the centres of slightly distorted octahedra, formed by phosphorus atoms (Fig. 3, grey polyhedra), Pt1 and Pt3 atoms also have octahedral coordination, but now the axial positions are occupied by the AE atoms, which leads to the expansion and severe distortion of the octahedra (Fig. 3, light blue and dark blue polyhedra). Distorted octahedra are connected to each other in the framework via common vertices. The Ca - Pt distances range from 2.79 to 2.94 Å.

Fig. 4 shows the AE-Pt distances for all known to date representatives of the $BaPt_4As_6$ structure type. It should be noted that all these distances are much shorter than the sum of the respective covalent radii (d (Ca–Pt) = 3.12 Å, d (Sr–Pt) = 3.31 Å, d (Ba–Pt) = 3.51 Å [34]). Since the Pn_2 dumbbell replacement occurs without the notable expansion of platinum-phosphorus framework, so the bond lengths practically do not change in ternary pnictides as compared to the binary ones, which is also supported by distances in the $CaPt_4P_6$ structure, then the reason for the very short AE - platinum contact formation, according to the authors of [17], is in the "matrix limitation". Increasing the AE - Pt distances would likely lead to the unfavorable lengthening of the bonds forming the covalent framework and a significant loss of stability.

As suggested in Ref. [17], this is the probably the reason why there is no $BaPt_4P_6$ compound, because the void size cannot accommodate large barium with the structure remaining stable. Evidently, in the case of barium, it is more favorable for the structure to be rearranged, and the

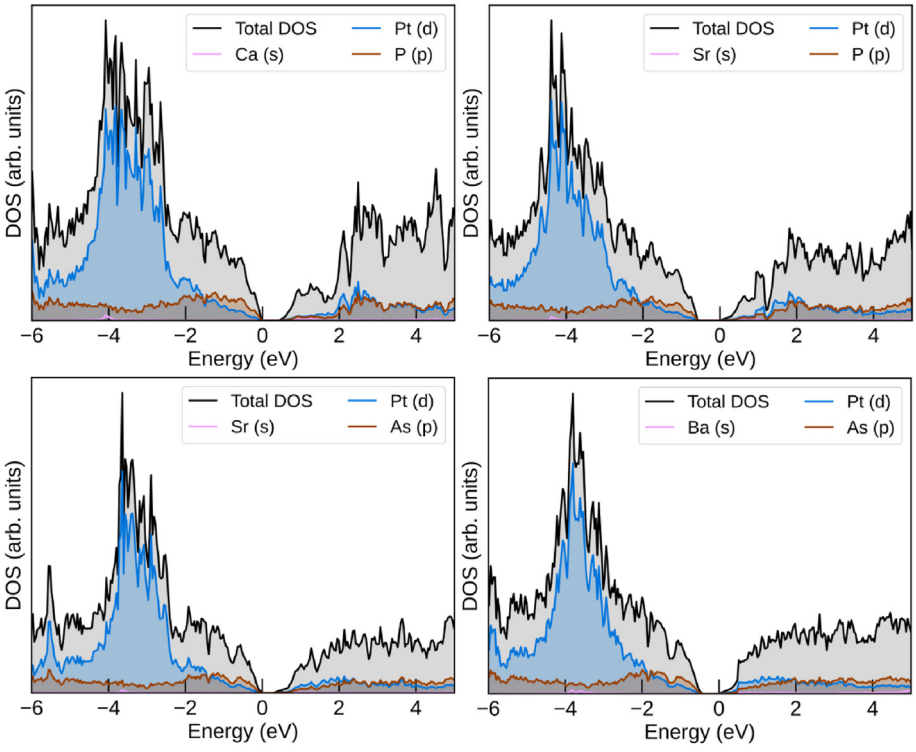

Fig. 5. Calculated total and projected densities of states (DOS) for $AEPt_4P_6$ (AE = Ca, Sr) (*top row*) and $AEPt_4As_6$ (AE = Sr, Ba) (*bottom row*).

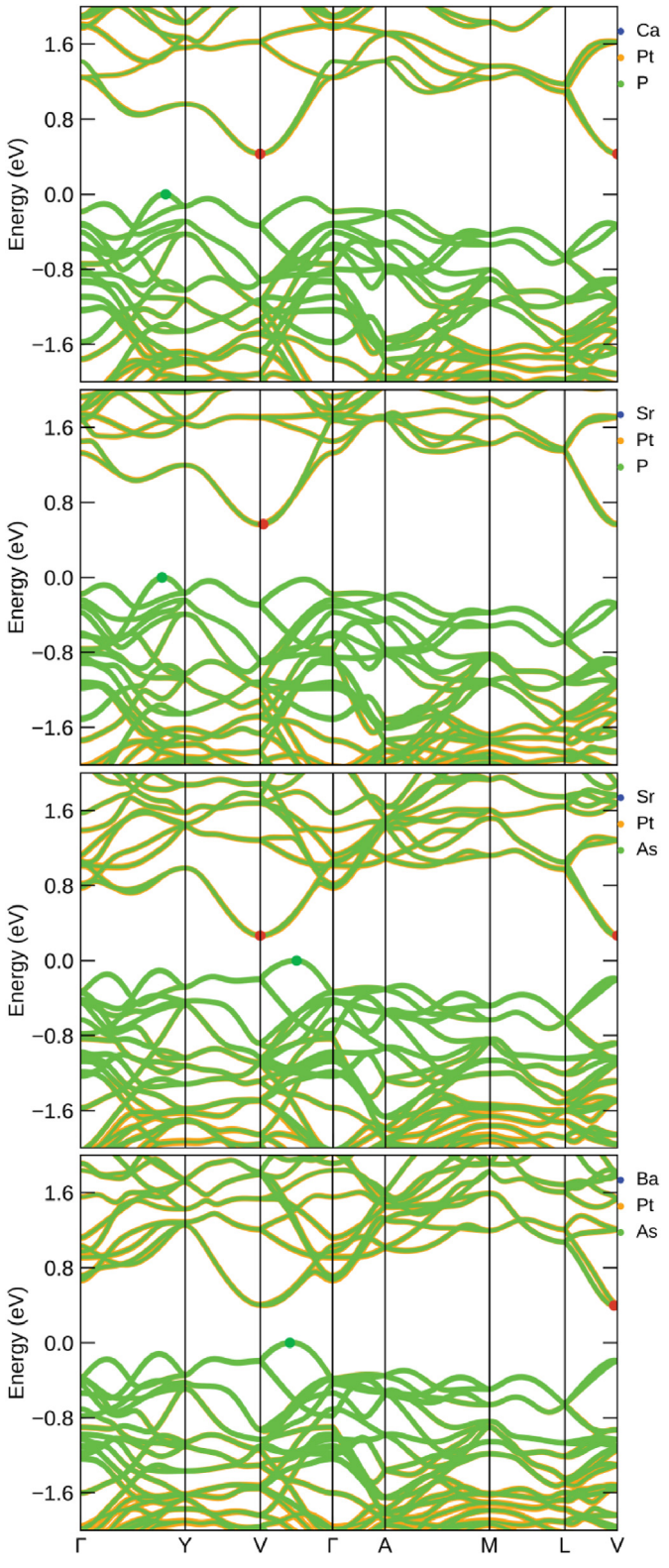

Fig. 6. Calculated band structure near the Fermi level for (top to bottom) $AEPt_4P_6$ (AE = Ca, Sr) and $AEPt_4As_6$ (AE = Sr, Ba). Atomic contributions to the respective bands are marked by the colors displayed in the legend. Red and greed dots denote Conduction Band Minimum (CBM) and Valence Band Maximum (VBM), respectively.

Table 4
Calculated Bader charges for $AEPt_4P_6$ (AE = Ca, Sr) and $AEPt_4As_6$ (AE = Sr, Ba).

	$CaPt_4P_6$	$SrPt_4P_6$	$SrPt_4As_6$	$BaPt_4As_6$
Pt	−0.06[a]; −0.37	−0.08[a]; −0.34	−0.37[a]; −0.58	−0.36[a]; −0.53
Pn	−0.03–0.07	−0.04–0.08	+0.09	+0.09
AE	+1.46	+1.44	+1.48	+1.37

[a] - Pt2 position.

$BaPt_2P_3$ compound is formed, which is also derived from the structure of pyrite, but it no longer features short Ba–Pt contacts. Since we found a new phosphide $CaPt_4P_6$ in the Ca–Pt–P system, we can assume that a similar one might exist in the Ca–Pt–As system as well.

To put the title compound in the proper context, we must emphasize that $CaPt_4P_6$ is rather unique for its ternary system. Only a few compounds are known in Ca–Pt–P system: CaPtP [35], which crystallizes in its own structure type, and also several non-stoichiometric compounds of the $CaPt_{1-x}P_{1+x}$ composition belonging to family of AlB_2-type structures [35]; $CaPt_2P_{1.43}$ ($BaPd_2As_2$ structure type) [36]; $CaPt_3P$ ($BaAu_3Ge$ structure type) [37], and $CaPt_8P_2$ ($DyPt_8P_2$ structure type) [38]. However, all these compounds are i) metal-rich and contain no more than 50 atomic % of phosphorus, and ii) do not have P–P bonds. In addition, all the compounds mentioned above can be described as frameworks based on the Pt–Pt and Pt–P contacts, whereas in the title compound there are no Pt–Pt bonding distances and the framework is based on Pt–P and P–P interactions. More detailed information on the bonding patterns will be provided in Section 3.2.

If we consider the polyhedra formed around the phosphorus atoms in all these compounds, in CaPtP each phosphorus is surrounded by three platinum atoms, and in the structure the planes of platinum and phosphorus atoms alternate with those of calcium atoms [35]. In $CaPt_2P_{1.43}$ phosphorus has two positions: the first is coordinated tetrahedrally by platinum atoms to form an antifluorite layer, and the second is located in the centres of square pyramids formed by platinum atoms [36]. Very similar pyramids are observed in $CaPt_3P$ and $CaPt_8P_2$ structures, albeit somewhat distorted [37,38].

Also, it is necessary to note, that in other compounds reported in the Ca–Pt–P system, the first coordination sphere of calcium atoms includes both phosphorus and platinum atoms, whereas in structure $CaPt_4P_6$ only platinum atoms make the nearest environment of calcium atoms. In addition, other compounds do not have very short (less than the sum of the covalent radii, which is 3.12 Å [34]) Ca–Pt distances that are present in the new ternary phosphide.

3.2. *Electronic structure and bonding*

Calculated total and projected DOS near the Fermi level and band structures for $AEPt_4P_6$ (AE = Ca, Sr) and $AEPt_4As_6$ (AE = Sr, Ba) are shown in Figs. 5 and 6, respectively. As seen from the plots, all the compounds are narrow-gap semiconductors with an indirect gap, calculated gap values are: 0.43 eV ($CaPt_4P_6$), 0.57 eV ($SrPt_4P_6$), 0.27 eV ($SrPt_4As_6$), and 0.40 eV ($BaPt_4As_6$). In all the compounds, top of the valence band and bottom of the conduction band consist of the mixture of Pt 5*d*-states and pnictogen *p*-states, while AE atoms do not contribute to the states close to the Fermi level and most likely exist as AE^{2+} cations.

For each pnictogen, we observe an increase of the gap by almost the same value (0.13–0.14 eV) moving from smaller to larger AE cation, while from P to As we observe a decrease in the band gap, which is consistent with more diffuse nature of the As 4*p*-states. Also, we observe the change in the VBM position: while for the phosphorus-based compounds it is between Γ and Y, for the arsenic-based ones it is between Γ and V.

In order to gain more insight into the bonding in the $AEPt_4P_6$ compounds, we have performed both direct-space (charge density, ELF) and orbital-space (COHP) analyses. Calculated Bader QTAIM charges are listed in Table 4. As seen from the table, there is prominent charge separation into AE cations with effective charge near +1.5 (slightly less for Ba), which is close to what one expects from formal AE^{2+} in such surroundings, Pt ions with negative charges grouped into two, smaller and larger, depending on whether there is an AE cation in the coordination polyhedron or not: Pt2, which has only Pn atoms in the coordination sphere, carries much lesser negative charge than Pt1 and Pt3. It is almost neutral in the phospides, and becomes notably more negative in the arsenides (see Table 4). Pnictogen atoms carry very small negative (P) or positive (As) charge, there is also a certain range depending on the particular environment, but it is far less pronounced than for Pt and we chose not to provide separate charges for each atom. Charge density distribution allows us to assume fairly strong covalency between the pnictogen atoms, polar interactions of mixed covalent and ionic nature between Pt and P, and no covalency between AE and Pt. This picture is further corroborated by the integrated partial Crystal Orbital Hamilton Population (IpCOHP) values, which can be considered a certain measure of covalent bond strength (see Table 5). The figures calculated for atom pairs of various types clearly show us strong covalent bond between pnictogen atoms in the Pn_2 units, slightly stronger in terms of bond energy for phosphorus dumbbells. These interactions are by far the strongest, yet, it is obvious that the Pt-Pn interactions are also at least partially of a covalent nature, although on average their energy is almost twice as low. Moreover, unconventionally short AE-Pt distances also result in some kind of interactions, albeit with much much lower energy, almost negligible as compared to the energies of the Pn-Pn and Pn-P bonds.

Further studies using topological analysis of the Electron Localization Function corroborate this picture perfectly. For $CaPt_4P_6$ we observe two types of maxima in the ELF topology that can be assigned to covalent bonds: type 1 and type 2 (see Fig. 7). The first one corresponds to the covalent bond in the P_2 units, the second to the polar Pt-Pn bonds. The picture is very similar for other $AEPt_4Pn_6$, although for As-based ones it is revealed at slightly lower η values. Thus, our bonding analysis establishes these compounds as based on the framework of Pt-Pn and Pn-Pn interactions with AE cations in the voids. It must be noted, though, that since we observe covalency both within the Pn_2 units and between Pn_2 and Pt, from the chemical bonding point the Pn_2 units are not dumbbells in a strict sense but rather part of a framework, their separation is arbitrary and is only done for the convenience of the structure representation, and we only keep using the word "dumbbell" for the sake of tradition.

Table 5
Calculated IpCOHP (eV) for $AEPt_4P_6$ (AE = Ca, Sr) and $AEPt_4As_6$ (AE = Sr, Ba).

	$CaPt_4P_6$	$SrPt_4P_6$	$SrPt_4As_6$	$BaPt_4As_6$
Pt-Pn	−2.19–2.57	−2.25–2.58	−2.08–2.50	−2.09–2.46
Pn-Pn	−4.73–4.81	−4.68–5.18	−3.79–4.10	−3.70–4.11
AE-Pt	−0.12–0.21	−0.13–0.27	−0.10–0.22	−0.15–0.26

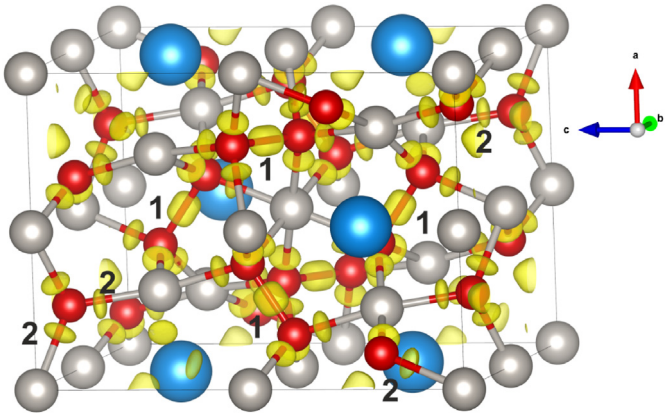

Fig. 7. ELF isosurface (η = 0.85; yellow) for the $CaPt_4P_6$ compound. Ca is light blue, P red, Pt grey. For the explanation of 1 and 2 see the text.

4. Conclusion

Using high-temperature route and lead as a flux, we have grown crystals and from the X-ray diffraction data determined the crystal structure of $CaPt_4P_6$, which is a first Ca-containing representative of the $BaPt_4As_6$ structure type. DFT calculations predict this compound to be an indirect gap semiconductor with the gap of ca 0.43 eV, which is similar to what our calculations predict for other members of the $AEPt_4Pn_6$ type. According to our bonding analysis in orbital (COHP) and direct (charge density, ELF) space, all these compounds consist of the covalent framework of Pn-Pn and Pt-Pn bonds, with AE cations filling the voids. From the point of chemical bond analysis, there is no reason to treat the Pn_2 units as separate dumbbells, as they are integral part of the covalent Pt-Pn 3D framework.

CRediT authorship contribution statement

Anastasiya Yu Makhaneva: Conceptualization, Investigation, Writing – original draft, Visualization. **Elena Yu Zakharova:** Methodology. **Sergey N. Nesterenko:** Investigation. **Konstantin A. Lyssenko:** Investigation, Formal analysis. **Alexey N. Kuznetsov:** Supervision, Investigation, Writing – original draft, Writing – review & editing, Visualization, Funding acquisition.

Declaration of competing interest

The authors declare the following financial interests/personal relationships which may be considered as potential competing interests:

Alexey N. Kuznetsov reports financial support was provided by Russian Foundation for Basic Research.

Data availability

No data was used for the research described in the article.

Acknowledgments

This work was supported by RFBR and DFG (RFBR grant no. 21-53-12015 DFG). X-ray data was collected using the equipment provided by the MSU Development Programme.

Appendix A. Supplementary data

Supplementary data to this article can be found online at https://doi.org/10.1016/j.jssc.2023.123969.

References

[1] J.M. Cameron, R.W. Hughes, Y. Zhao, D.H. Gregory, Ternary and higher pnictides; prospects for new materials and applications, Chem. Soc. Rev. 40 (2011) 4099–4118, https://doi.org/10.1039/C0CS00132E.
[2] F. Hulliger, Crystal chemistry of the chalcogenides and pnictides of the transition elements, Struct. Bonding (Berlin) 4 (2008) 83–229, https://doi.org/10.1007/BFb0119186.
[3] H.F. Franzen, Structure and bonding in metal-rich compounds: pnictides, chalcides and halides, Prog. Solid State Chem. 12 (1978) 1–39, https://doi.org/10.1016/0079-6786(78)90002-X.
[4] S.T. Oyama, T. Gott, H. Zhao, Y.K. Lee, Transition metal phosphide hydroprocessing catalysts: a review, Catal. Today 143 (2009) 94–107, https://doi.org/10.1016/j.cattod.2008.09.019.
[5] P. Xiao, W. Chen, X. Wang, A review of phosphide-based materials for electrocatalytic hydrogen evolution, Adv. Energy Mater. 5 (2015), 1500985, https://doi.org/10.1002/aenm.201500985.

[6] M. Sun, H. Liu, J. Qu, J. Li, Earth-rich transition metal phosphide for energy conversion and storage, Adv. Energy Mater. 6 (2016), 1600087, https://doi.org/10.1002/aenm.201600087.

[7] R. Prins, M.E. Bussell, Metal phosphides: preparation, characterization and catalytic reactivity, Catal letters 142 (2012) 1413–1436, https://doi.org/10.1007/s10562-012-0929-7.

[8] M.R. Norman, High-temperature superconductivity in the iron pnictides, Physics 1 (2008) 21, https://doi.org/10.1103/Physics.1.21.

[9] Q. Si, R. Yu, E. Abrahams, High-temperature superconductivity in iron pnictides and chalcogenides, Nat. Rev. Mater. 1 (2016) 1–15, https://doi.org/10.1038/natrevmats.2016.17.

[10] R. Pöttgen, W. Hönle, H.G. von Schnering, Phosphides, Solid state chemistry, in: R.B. King (Ed.), Encyclopedia of Inorganic Chemistry, VII, second ed., Wiley, New York, 2005, pp. 4255–4308, https://doi.org/10.1002/0470862106.ia184.

[11] H.G. Von Schnering, W. Hönle, Chemistry and structural chemistry of phosphides and polyphosphides. 48. Bridging chasms with polyphosphides, Chem. Rev. 88 (1988) 243–273, https://doi.org/10.1021/cr00083a012.

[12] W. Jeitschko, M.H. Möller, Phosphides and polyphosphides of the transition metals, Phosphorus, Sulfur, Silicon Relat. Elem. 30 (1987) 413–416, https://doi.org/10.1080/03086648708080608.

[13] A.Y. Makhaneva, E.Y. Zakharova, S.N. Nesterenko, K.A. Lyssenko, V.O. Yapaskurt, A.N. Kuznetsov, Metal-rich phosphides obtained from the lead flux: synthesis, crystal, and electronic structure of $Sr_5Pt_{12}P_9$ and $BaPt_3P_2$, Inorg. Chem. 61 (2022) 9173–9183, https://doi.org/10.1021/acs.inorgchem.2c00747.

[14] D. Johrendt, A. Mewis, BaPdP, Ba_2PdP_3, and $BaPd_2P_4$ - Zintl compounds or intermetallic phases? J. Alloys Compd. 205 (1994) 183–189, https://doi.org/10.1016/0925-8388(94)90787-0.

[15] J.A. Dolyniuk, J. Wang, K. Lee, K. Kovnir, Twisted Kelvin cells and truncated octahedral cages in the crystal structures of unconventional clathrates, AM_2P_4 (A= Sr, Ba; M= Cu, Ni), Chem. Mater. 27 (2015) 4476–4484, https://doi.org/10.1021/acs.chemmater.5b01592.

[16] V. Keimes, D. Johrendt, A. Mewis, $BaNi_2P_4$: dimorphism by peierls instability? Z. Anorg. Allg. Chem. 621 (1995) 925–930, https://doi.org/10.1002/zaac.19956210603.

[17] G. Wenski, A. Mewis, Ternary pyrite-type derivatives: preparation and crystal structure of $SrPt_4P_6$, $SrPt_4As_6$, $BaPt_4As_6$ and $BaPt_2P_3$, Z. Naturforsch. B Chem. Sci. 42 (1987) 507–513, https://doi.org/10.1515/znb-1987-0419.

[18] A.Yu Makhaneva, E.Yu Zakharova, S.N. Nesterenko, K.A. Lyssenko, A.N. Kuznetsov, Merging the $AuCu_3$- and $BaAl_4$-based structure motifs: flux-assisted synthesis, crystal, and electronic structure of $Ca_2Pt_7XP_{4-\delta}$ phosphide platinides (X=Al, Ti, and Zn), Dalton Trans. 51 (2022) 18583–18592, 10.1039/d2dt03367d.

[19] SAINT, Version 8.40B, Bruker AXS Inc., Madison, Wisconsin, USA, 2017.

[20] L. Krause, R. Herbst-Irmer, G.M. Sheldrick, D. Stalke, Comparison of silver and molybdenum microfocus X-ray sources for single-crystal structure determination, J. Appl. Crystallogr. 48 (2015) 3–10, https://doi.org/10.1107/S1600576714022985.

[21] G.M. Sheldrick, SHELX-2018/3, Program Package for Crystal Structure Solution and Refinement, Göttingen, Germany, 2018.

[22] G. Kresse, D. Joubert, From ultrasoft pseudopotentials to the projector augmented-wave method, Phys. Rev. B 59 (1999) 1758–1775, https://doi.org/10.1103/PhysRevB.59.1758.

[23] G. Kresse, J. Furthmüller, Vienna Ab initio simulation package (VASP), v.5.4.4, http://www.vasp.at/.

[24] J.W. Furness, A.D. Kaplan, J. Ning, J.P. Perdew, J. Sun, Accurate and numerically efficient r2SCAN meta-generalized gradient approximation, J. Phys. Chem. Lett. 11 (2020) 8208–8215, https://doi.org/10.1021/acs.jpclett.0c02405.

[25] r^2SCAN subroutines, Repository for subroutines/patches needed to implement r2SCAN in popular electronic structure codes. https://gitlab.com/dhamil/r2scan-subroutines/-/tree/master.

[26] T. Lu, F. Chen, Multiwfn: a multifunctional wavefunction analyzer, J. Comput. Chem. 33 (2012) 580–592, https://doi.org/10.1002/jcc.22885.

[27] K. Momma, F. Izumi, VESTA 3 for three-dimensional visualization of crystal, volumetric and morphology data, J. Appl. Crystallogr. 44 (2011) 1272–1276, https://doi.org/10.1107/S0021889811038970.

[28] A.M. Ganose, A.J. Jackson, D.O. Scanlon, sumo: command-line tools for plotting and analysis of periodic ab initio calculations, J. Open Source Softw. 3 (2018) 717–719, https://doi.org/10.21105/joss.00717.

[29] R. Dronskowski, P.E. Blöchl, Crystal orbital Hamilton populations (COHP). Energy-resolved visualization of chemical bonding in solids based on density-functional calculations, J. Phys. Chem. 97 (1993) 8617–8624, https://doi.org/10.1021/j100135a014.

[30] V.L. Deringer, A.L. Tchougreeff, R. Dronskowski, Crystal orbital Hamilton population (COHP) analysis as projected from plane-wave basis sets, J. Phys. Chem. A 115 (2011) 5461–5466, https://doi.org/10.1021/jp202489s.

[31] S. Maintz, V.L. Deringer, A.L. Tchougreeff, R. Dronskowski, Analytic projection from plane-wave and PAW wavefunctions and application to chemical-bonding analysis in solids, J. Comput. Chem. 34 (2013) 2557–2567, https://doi.org/10.1002/jcc.23424.

[32] S. Maintz, V.L. Deringer, A.L. Tchougréeff, R. Dronskowski, LOBSTER: a tool to extract chemical bonding from plane-wave based DFT, J. Comput. Chem. 37 (2016) 1030–1035, https://doi.org/10.1002/jcc.24300.

[33] A. Baghdadi, A. Finley, P.A. Russo, R.J. Arnott, A. Wold, Crystal growth and characterization of PtP_2, J. Less Common. Met. 34 (1974) 31–38, https://doi.org/10.1016/0022-5088(74)90214-8.

[34] B. Cordero, V. Gómez, A.E. Platero-Prats, M. Revés, J. Echeverría, E. Cremades, F. Barragán, S. Alvarez, Covalent radii revisited, Dalton Trans. 21 (2008) 2832–2838, https://doi.org/10.1039/B801115J.

[35] G. Wenski, A. Mewis, Ternäre Varianten des AlB_2-Typs. Darstellung und Struktur von Ca(Eu)PtX (X= P, As, Sb), $CaPt_xP_{2-x}$, $EuPt_xP(As)_{2-x}$ und $CaPt_xAs_{0,9}$, Z. Anorg. Allg. Chem. 543 (1986) 49–62, https://doi.org/10.1002/zaac.19865431206.

[36] G. Wenski, A. Mewis, $BaAl_4$-Denvative structures of ARu_2X_2 (A= Ca, Sr, Ba. Eu; X= P, as) and of APt_2P_{2-x} (A= Ca, Eu), Z. Naturforsch. B Chem. Sci. 41 (1986) 38–43, https://doi.org/10.1515/znb-1986-0108.

[37] A. Subedi, L. Ortenzi, L. Boeri, Electron-phonon superconductivity in APt_3P (A= Sr, Ca, La) compounds: from weak to strong coupling, Phys. Rev. B 87 (2013), 144504, https://doi.org/10.1103/PhysRevB.87.144504.

[38] X. Gui, Z. Sobczak, T. Klimczuk, W. Xie, Pt-rich intermetallic APt_8P_2 (A= Ca and La), J. Alloys Compd. 798 (2019) 53–58, https://doi.org/10.1016/j.jallcom.2019.05.239.